DEVELOPMENT AND VALIDATION OF A CHARACTERISTIC BOUNDARY CONDITION FOR A CELL-CENTERED EULER METHOD *)

J.I. van den Berg, J.W. Boerstoel,
National Aerospace Laboratory NLR,
Amsterdam, the Netherlands.

Abstract

The development and numerical validation of a solid-wall boundary condition is presented for the numerical solution of the Euler equations with a cell-centered central-difference scheme. This solid-wall boundary condition was obtained from the theory of characteristics, and was also formulated for a cell-centered central-difference scheme. The boundary condition was developed to clarify the question what the effect is of various boundary-condition algorithms on the accuracy of the 3D numerical solution of the Euler equations.

The numerical validation of the solid-wall boundary condition consists of a comparison of results obtained with the conventional- and the new solid-wall boundary condition. Also discretization and convergence errors as well as grid dependency of the solution were investigated.
As a test case, the NLR 7301 airfoil was chosen. Calculations were performed for the supercritical, shock-free flow at $M_\infty = 0.721$, $\alpha = -0.194^\circ$, and for a flow with a strong shock at $M_\infty = 0.70$, $\alpha = 2.0^\circ$.

1. Introduction

The main subject of this paper is a study into the effects of the solid-wall boundary condition on the accuracy of the numerical solution of the 3D Euler equations around aerodynamic configurations. The motivation of this study lies in the application of the Euler equations to the flow around delta wings[1]. Here accuracy plays an important role in the simulation of the vortical flow due to separation from sharp edges.
In Euler methods, the conventional boundary condition along a solid wall is the prescription of a normal velocity component of zero and a second order accurate extrapolation of the static pressure towards the wall. This leads to a false, numerical, entropy layer along the surface. This entropy layer can affect the accuracy of the inviscid-flow solution and could render future extensions to viscous-flow simulations useless. Also the false entropy layers can have a large effect on the flow separation from sharp edges, i.e. at the trailing edge and at the leading edge of a delta wing with leading edge vortices.
The following items, that have effect on the accuracy of the numerical solution, will be discussed:

- solid-wall boundary condition algorithm,
- grid-quality and grid-resolution,
- location of the far-field boundary,
- (boundary conditions of the) artificial dissipation operator.

The solid-wall boundary condition presented in this paper, called characteristic solid-wall boundary condition, is obtained from the theory of characteristics.
In Ref. 2. , a theoretical analysis of the consistency, well-posedness and stability of the characteristic boundary condition is described. Here we will focus on the numerical analysis of this boundary condition. The results and conclusions, presented in this paper, are obtained from two-dimensional airfoil flow.
As a test case we use the NLR 7301 airfoil, for the so-called supercritical shock-free flow (design condition) at $M_\infty = 0.721$, $\alpha = -0.194^\circ$. Also calculations have been carried out for a flow at $M_\infty = 0.70$, $\alpha = 2.0^\circ$. For this latter case a strong shock is present at the upper side of the airfoil.

The Euler equations for conservation of momentum, mass and energy, are discretized by a fully conservative cell-centered central-difference scheme, and solved numerically using a 4-stage Runge-Kutta time integration scheme[3]. The characteristic solid-wall boundary condition is also formulated with a cell-centered central-difference scheme.
The NLR information system for the 3D Euler method has been used for this study[4,5,6,7]. It consists of (c.f. Fig. 1):

- subsystems for geometry processing, grid generation, flow calculation, flow visualization and data processing,
- subsystems for method management and data management.

2. Governing equations

2.1 Discretization of the conservation equations

The governing equations form a set of five coupled non-linear first-order hyperbolic partial differential equations describing the conservation of mass, of momentum, and of energy for the inviscid flow of an ideal gas, i.e. in a Cartesian coordinate system:

$$U_t + F_x + G_y + H_z = 0, \qquad (2.1)$$

where U is the flow state vector,

$$U = [\,\rho,\ \rho u,\ \rho v,\ \rho w,\ \rho E]^T, \qquad (2.2)$$

and F,G,H are the flux vectors, in Cartesian coordinates:

$$[F,G,H]^T = \begin{bmatrix} \rho u & \rho v & \rho w \\ \rho u^2 + p & \rho uv & \rho uw \\ \rho uv & \rho v^2 + p & \rho vw \\ \rho uw & \rho vw & \rho w^2 + p \\ uH & vH & wH \end{bmatrix}^T, \qquad (2.3)$$

with

*) This research was partly performed under contract with the Netherlands Agency for Aerospace Programs (NIVR) for the Netherlands Ministry of Defence.

$(u,v,w)^T$ = the velocity vector,
ρ = the density,
p = the static pressure,
E = the total energy,

$$E = \frac{1}{\gamma-1}\frac{p}{\rho} + \tfrac{1}{2} q^2$$

H = the total enthalpy,

$$H = E + p = \frac{\gamma}{\gamma-1}\frac{p}{\rho} + \tfrac{1}{2} q^2$$

The equations are solved numerically with a cell-centered central-difference scheme. Artificial dissipative terms are added to the discretized conservation equations. They consist of a second-order term that should be active in shocks in order to create steep shocks, and a fourth-order term, active away from shocks to eliminate decoupling of the solution at odd and even grid points. A switch factor dependent on the second-order derivative of the pressure is used as sensor to detect shocks where the second-order dissipative term is switched on and the fourth order dissipative term is switched off[2,3].
The time integration of the discrete equations is performed with a 4-stage Runge-Kutta scheme. For each grid cell, the discrete conservation equations are written as

$$U_{ijk}^{(m+1)} = U_{ijk}^{n} - dt\ (Q_{ijk}^{(m)} - D_{ijk}^{n}) , \qquad (2.4)$$

where

U_{ijk}^{n} = the state vector at cell ijk at time level n ,

(m) = stage in Runge-Kutta scheme,

$m=0..3,\ U_{ijk}^{(0)} = U_{ijk}^{n},\ U_{ijk}^{(4)} = U_{ijk}^{n+1}$,

n = time level,

$Q_{ijk}^{(m)}$ = convective divergence at cell ijk at stage (m),

D_{ijk}^{n} = dissipative divergence at cell ijk at time level n ,

dt = Runge-Kutta time-step[2].

2.2 Boundary conditions

The discretization of the conservation equations with a cell-centered central-difference scheme requires the value of the flow state vector at each cell-centre of an extra layer of cells along the boundary, just outside the flow domain. The state vector in these so-called halo cells has to be determined from the boundary conditions. Here we will describe the solid-wall and far-field boundary conditions as implemented in the present Euler method.

2.2.1 Solid-wall boundary

Along the solid wall, the velocity vector tangential to the solid wall, the pressure and the total enthalpy are extrapolated linearly from the two cells adjacent to the wall towards the solid wall. The normal component of the velocity vector at the solid wall is set to zero. From this velocity vector, the pressure and the total enthalpy, the density along the solid wall can be calculated. The flow state vector in the centres of the halo cells is determined using an linear extrapolation formula[3].

2.2.2 Far-field boundary

At the far-field boundary, a boundary condition based on Riemann invariants for a one-dimensional flow normal to the boundary is used. Using the component of the velocity vector normal to the far-field boundary u_n and the speed of sound c, Riemann invariants corresponding to inflow and outflow can be determined. The incoming and outgoing Riemann invariants are respectively

$$Ri = u_n - \frac{2c}{\gamma-1} , \qquad (2.5)$$

$$Ro = u_n + \frac{2c}{\gamma-1} . \qquad (2.6)$$

Combining these Riemann invariants gives a description of the normal component of the velocity vector and speed of sound at the far-field boundary:

$$u_n = (Ri + Ro) / 2 , \qquad (2.7.a)$$

$$c = (\gamma-1) (Ri - Ro) / 4 . \qquad (2.7.b)$$

Depending on inflow or outflow, the state vector at the far-field boundary can be determined. For flow entering the flow domain ($u_n > 0.$), the tangential velocity components and the entropy (or more precise a measure for the entropy $S = p\rho^{-\gamma}$) are set to the free-stream values, Ro to the value obtained through extrapolation from the interior of the flow domain to the boundary; for flow leaving the flow domain ($u_n < 0.$), the tangential velocity components and entropy are set to the extrapolated values at the boundary, Ri to its free-stream value. In this way, the flow state vector at the far-field boundary is calculated. The flow state in the centre of the halo cell outside the flow domain is determined by extrapolation[3].

3. Characteristic solid-wall boundary condition

Along a solid-wall boundary, a layer of auxiliary cells of half a mesh height above the surface in the flow domain is introduced (Fig. 2). For each auxiliary cell a set of five semi-discrete conservation equations is defined,

$$(U_t)_{ij\frac{1}{2}} + Q_{ij\frac{3}{4}}(U^n) - D_{ij\frac{3}{4}}(U^n) = 0. \qquad (3.1)$$

where

$(U_t)_{ij\frac{1}{2}}$ = the time derivative of the state vector at the solid-wall ij½,

$Q_{ij\frac{3}{4}}(U^n)$ = the divergence of the convective fluxes, at the cell centre ij¾ of the auxiliary cell, at time level n,

$D_{ij\frac{3}{4}}(U^n)$ = the divergence of the dissipative fluxes at the cell centre ij¾ of the auxiliary cell, at time level n.

These equations are transformed into characteristic form. This transformation is performed by premultiplying the equations by the 5*5 matrix

$$T_{ij\frac{1}{2}} = R^{-1}_{ij\frac{1}{2}}\ C_{ij\frac{1}{2}}\ S_{ij\frac{1}{2}} . \qquad (3.2)$$

The 5x5 matrix S introduces a transformation from the (x,y,z) coordinate system to a local coordinate

system ($\underline{n},\underline{s},\underline{t}$), with $\underline{n}$ the unit normal to the cell face $ij_{\frac{1}{2}}$ on the boundary, and ($\underline{s},\underline{t}$) tangential to the surface along the boundary. C is a scaling matrix, scaling eigenvalues (velocities) to dimensionless quantities (Mach number). R^{-1} is the transformation of flow-state changes in primitive variables to flow-state changes in Riemann variables. This leads to

$$(\phi_t)_{ij\frac{1}{2}} + T_{ij\frac{1}{2}} [\, Q_{ij\frac{3}{4}}(U^n) - D_{ij\frac{3}{4}}(U^n) \,] = 0, \quad (3.3)$$

a set of five conservation equations. Here ϕ_t is the vector of time-derivatives of the Riemann-variables,

$$\phi_t = [\, r_t^+ , r_t^S , r_t^{t1}, r_t^{t2}, r_t^- \,], \quad (3.4)$$

where

$$r_t^+ = \rho\tilde{u}_t + \frac{1}{c} p_t ,$$
$$r_t^S = \frac{p}{cS} S_t ,$$
$$r_t^{t1} = \rho\tilde{v}_t ,$$
$$r_t^{t2} = \rho\tilde{w}_t ,$$
$$r_t^- = \rho\tilde{u}_t - \frac{1}{c} p_t ,$$

These time derivatives correspond to the eigenvalues $\lambda_1 = \tilde{u}+c$, $\lambda_2 = \lambda_3 = \lambda_4 = \tilde{u}$, and $\lambda_5 = \tilde{u}-c$, respectively. Furthermore,

- $\tilde{u}$ = velocity component in $\underline{n}$ direction (normal to the boundary, positive if $\tilde{u}$ is directed into the flow domain),
- $\tilde{v},\tilde{w}$ = velocity components tangential to the boundary,
- c = speed of sound,
- S = p/ρ^{γ} , a variable depending on the entropy.

Time derivatives of the Riemann variables representing information entering the flow domain through the boundary can now be replaced by boundary conditions. They can be recognized by a negative sign of the corresponding eigenvalue.
At the solid wall, a boundary condition has to be prescribed for r_t^- .The boundary condition is : the normal component of the velocity vector must tend to zero, when time goes to infinity.
For the Riemann variables with the zero eigenvalues ($\lambda_2 = \lambda_3 = \lambda_4 = 0$), it is permitted to prescribe boundary conditions but it is not necessary. Physically the three corresponding conservation equations for r_t^S, r_t^{t1}, r_t^{t2} , describe the transport of entropy and momentum in a direction tangential to the solid wall.
From numerical experiments with transonic shock-free flows around airfoils, it was concluded that it is useful to apply also a boundary condition for the Riemann variable r_t^S. The boundary condition chosen in the present work is that the entropy gradient in the direction normal to the solid wall vanishes at the solid wall, when time goes to infinity (steady state).
These two boundary conditions can be expressed as:

$$(r_t^-)_B = - d_{uB}\, \rho_B (\, \tilde{u}_B - \tilde{u}_{oB} \,) / \Delta t_B - (r_t^+)_B \quad (3.5.a)$$
$$(r_t^S)_B = - d_S \left(\frac{p}{cS}\right)_B (\, S_B - S_{oB} \,) / \Delta t_B \quad (3.5.b)$$

where subscript B denotes the multi-index on the solid-wall boundary,

$$.B = .ij_{\frac{1}{2}} .$$

Using $r_t^+ + r_t^- = 2\rho\,(\tilde{u}_t)_B$, and giving prescriptions that drive $(\tilde{u}_t)_B$ and $(S_t)_B$ to zero, gives the desired boundary conditions,

- $\tilde{u}_B$ = actual value of normal velocity at cell-face centre B,
- $\tilde{u}_{oB}$ = desired value of normal velocity at cell-face centre B,
- S_B = actual value of entropy at cell-face centre B,
- S_{oB} = desired value of entropy at cell-face centre B, $S_{oB} = S_{ij1}$,
- d_{uB} , d_S scaling parameters (> 0), specifying how fast $\tilde{u}_{oB}$, and S_{oB} are driven to their desired values $\tilde{u}_{oB}$, S_{oB} when $t \longrightarrow \infty$.

These boundary conditions may be written in the general form,

$$(\phi_t)_B + f_B(U^n) = 0. \quad (3.6)$$

This is a set of five equations, two of them are the boundary conditions (3.5), the remaining three can be arbitrarily defined, because they are eliminated, see below.
Of the five conservation equations (3.3), two equations have been replaced by boundary conditions. The remaining three equations are also required to obtain a total of five difference equations for the flow-state vector at each halo cell centre. They are called auxiliary equations. These auxiliary equations are thus semi-discretized conservation equations.
The boundary-condition equations (3.6) and the remaining auxiliary equations are combined to a set of five new equations, by a so-called incidence matrix I_B. It is defined as a diagonal matrix whose elements are 0 for Riemann variables which corresponding conservation equation has been replaced by a boundary condition, and 1 for the other Riemann variables. In our case $I_B = \mathrm{diag}(1,0,1,1,0)$.
Now the boundary conditions and conservation equations can be combined using the incidence matrix,

$$(\phi_t)_B + I_B\, T_B [\, Q_{ij\frac{3}{4}}(U^n) - D_{ij\frac{3}{4}}(U^n) \,] + (I-I_B)\, f_B(U^n) = 0. \quad (3.7)$$

This set of equations is mapped back into equations for the primitive state vector $U_{ij\frac{1}{2}}$ at the solid wall by pre-multiplying with the matrix T_B^{-1}.

4. Numerical analysis of boundary conditions

4.1 Description of test cases

As a test case the NLR 7301 airfoil was chosen. It was designed for the free-stream flow condition $M_\infty = 0.721$, $\alpha = -0.194^\circ$, to have a so-called super-critical shock-free flow, i.e. the flow has supersonic and subsonic regions but no shock. This

is a widely used and critical test case for the numerical validation of Euler codes.
Also calculations were performed for the free-stream condition $M_\infty = 0.7$, $\alpha = 2.0^\circ$, for which the flow features a strong shock on the upper side of the airfoil.

For the calculations two grids were used. All are 1-block O-type grids, and can be characterized by the number of grid points along the surface, the number of grid points in the direction normal to the surface, the cell-aspect ratio at the solid wall, the cell-aspect ratio at the far-field boundary, and the location of the far-field boundary. The cell aspect ratio is defined as the height of the cell (normal to the boundary) divided by the cell length (along the boundary). Table 1 provides a list of the grids.
Grid A (depicted in Fig. 3) has 256x160 cells on its finest level (256 cells along the airfoil, 160 in the direction normal to the surface), and a cell-aspect ratio of 1.0 at the solid wall, 2.0 at the far-field boundary, located 100 chords from the airfoil.
Grid B is similar to grid A, but with the far-field boundary located 40 chords from the airfoil, requiring 128 cells in direction normal to the surface.
Unless otherwise stated, each computation result is fully converged, i.e starting from a uniform flow condition as initial solution, the residue was decreased at least four orders of magnitude.

4.2 Results NLR 7301 airfoil, M_∞=0.721, α=-0.194°

For this super-critical shock-free flow condition the results with the Euler method obtained on grid A are discussed.
Results calculated with the characteristic solid-wall boundary condition were compared to results obtained with the conventional solid-wall boundary condition of a zero normal velocity component and extrapolation of the pressure.
In Fig. 4. the Mach number distribution in the flow field around the airfoil is given. As can be seen, there is a sonic line (Mach=1.), a subsonic region and a supersonic region but no shock. Comparison of the Mach number distribution along the surface obtained with the characteristic solid-wall boundary condition, and with that from hodograph theory[8], figure 5, shows an exellent agreement, except at the upper side of the airfoil where there is a slight difference. This is near the point of the highest curvature of the airfoil, where small inaccuracies due to the artificial dissipative terms in the Euler method are locally largest.
The result for the Euler method with conventional solid-wall boundary condition is quite similar to the result shown in Fig. 4. This is clear from figure 6, which shows the Mach number distribution on the surface for the Euler method with the characteristic solid-wall boundary condition, for the one with the conventional solid-wall boundary condition and for the hodograph theory[8]. Only slight differences can be observed.
For inviscid shock-free flow, the flow should be isentropic and any production of entropy or total pressure is a numerical, non-physical artifact. The increase in entropy, here defined as $S - S_\infty = c_v \log((p/\rho^\gamma)*(p_\infty/\rho_\infty^\gamma))$, at the surface of the airfoil of both calculations are compared to each other in Fig. 7. In case of the characteristic solid-wall boundary condition, the numerical entropy layer has been reduced by a factor of approximately two compared to the result for the conventional boundary condition. In this case, the entropy increase is negligable at the lower side, and small and almost constant at the upper side. Only near the stagnation point an increase of entropy can be observed. A study into the source of this entropy 'bubble' led to the conclusion that it is due to discretization errors.

It was not possible to obtain a shock-free solution on grid B, while the only difference between grid A and grid B is the location of the far-field boundary. We therefore conclude that, for the spatial discretization techniques in the Euler method applied here, there is insufficient resolution to describe the shock-free flow solution accurately.

4.3 Results NLR 7301 airfoil, M_∞=0.70, α=2.0°

For this test case with a strong shock on the upper side of the airfoil, very similar solutions were obtained on grid A and grid B.
In figure 8, the Mach number distribution in the flow field around the airfoil is given, as calculated on grid A using the Euler method with the characteristic solid-wall boundary condition. In figure 9 the Mach number distribution along the surface is given as computed on both grids using the Euler method with the characteristic solid-wall boundary condition. The effect of the grid on the position of the shock is negligable, only a slight shift can be observed. Also the strength of the shock is not influenced.
The reason that it is possible to arrive at a converged satisfactory solution on grid B in case of a strong shock, while it was not possible in case of the shock-free super-critical flow, can be explained by observing that shock-free super-critical airfoil flows are extremely sensitive to numerical errors of all kinds, as follows. At the downstream side of a supersonic pocket, the flow decellerates smoothly through a sonic line from supersonic to subsonic flow. This decelleration is thus not discontinuously through a shock, as is usually the case. Now small disturbances generated anywhere in the supersonic field or at its boundary, are propagated along characteristics, and reflected repeatedly against the airfoil and at the sonic line. These reflected disturbances pile up near the downstream foot of the sonic line on the airfoil, and tend to destroy there the shock-free character of the flow. When these disturbances (numerical approximation errors generated everywhere in the supersonic pocket) are small, their combined effect will thus become visible as a change of the shock-free flow at the foot of the sonic line, often to a flow with a small shock.
Here we will discuss the results as obtained on grid A using the Euler method with the characteristic and the conventional solid-wall boundary condition. In figure 10 the Mach number distributions along the surface of both calculations are compared to each other. They coincide within plotting accuracy. In figure 11 the increase in entropy along the surface of both boundary conditions are compared to each other. It is seen that, in case of the characteristic solid-wall boundary condition, along the lower surface, the flow is nearly isentropic for both boundary conditions, except near the stagnation point. At the upper surface, errors in the entropy have been approximately halved, compared to the errors with the conventional solid-wall boundary condition.

5. Concluding remarks.

The characteristic solid-wall boundary condition leads, in terms of the numerical entropy layer, to a more accurate numerical solution of the Euler method than the frequently used standard boundary condition involving the zero normal velocity component and extrapolation of the pressure towards the solid wall.

For the very sensitive test case with the shock-free flow, the location of the far field boundary appeared to be of importance. Further study of the grid dependence of the solution is required.

It appeared that the rate of convergence is not influenced when the conventional solid-wall boundary condition is replaced by the characteristic solid-wall boundary condition. The concept of the characteristic solid-wall boundary condition offers, at least in principle, through utilizing the possibility to impose additional boundary conditions, the opportunity to simulate smooth body separation such as secondary flow separation in delta wing vortex flow simulations.

6. References.

[1] JACOBS,J.M.J.W. ,HOEIJMAKERS,H.W.M. : "Aspects of the application of an Euler-equation method to the simulation of leading edge vortex flow .", NLR TP 89272 L ;
also Proceedings Eighth GAMM Conference on Numerical Methods in Fluid Mechanics, 27-29 september 1989, Delft, The Netherlands.

[2] VAN DEN BERG,J.I. ,BOERSTOEL,J.W. :"Theoretical and numerical investigation of characteristic boundary conditions for cell-centered Euler flow calculations.", NLR TR 88124 L.

[3] JAMESON,A. ,SCHMIDT,W. :"Recent developments in numerical methods for transonic flows.", Computer Methods in Applied Mechanics and Engineering 51, (1985), pp. 407-463.

[4] BOERSTOEL,J.W. :"Progress report of the development of a system for the numerical simulation of Euler flows, with results of preliminary 3D propellor-slipstream/exhaust-jet calculations.", NLR TR 88008 L.

[5] BOERSTOEL,J.W. et al.:"Design and testing of a multiblock grid-generation procedure for aircraft design and research.", NLR TP 89146 L.

[6] BUYSEN,F.A. :"Flow visualisation at NLR : VISU3D ", NLR TP 89317.

[7] SCHUURMAN,J.J. ,KASSIES,A. ,MEELKER,J.H. : "Method Management for the benefit of large software packages for analyses in CAE.", NLR TP 89027.

[8] YOSHIHARA,H. , SACHER,P. (ed.) :"Test cases for inviscid flow field methods.", Advisitory Report 211, AGARD-AR-211, 1985.

GRIDS	A	B
o number of cells along airfoil	256	256
o number of cells in normal direction	160	128
o cell-aspect ratio at solid-wall	1.0	1.0
o cell-aspect ratio at outer boundary	2.0	2.0
o location of outer boundary	100c	40c

Table 1. Characteristics of the grids used.

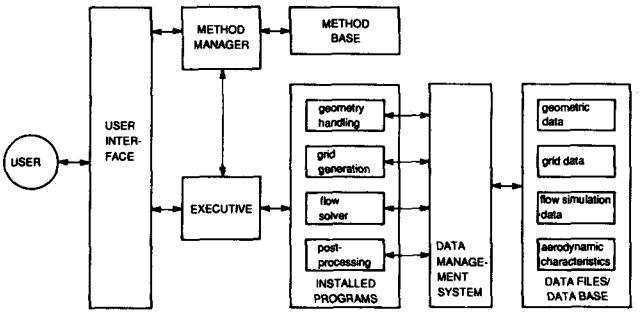

Fig. 1. Conceptual design of an information system for flow simulation.

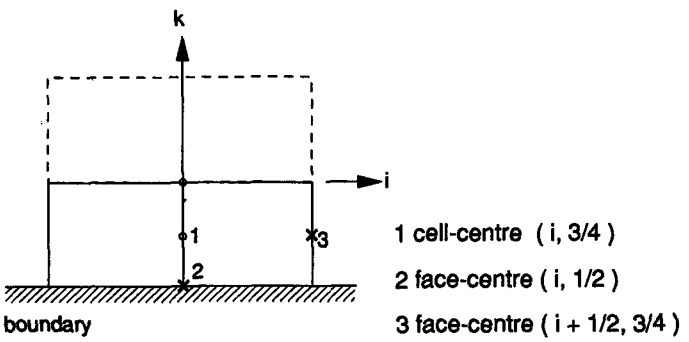

Fig. 2. Auxiliary cell (2D) along the boundary of the computational domain.

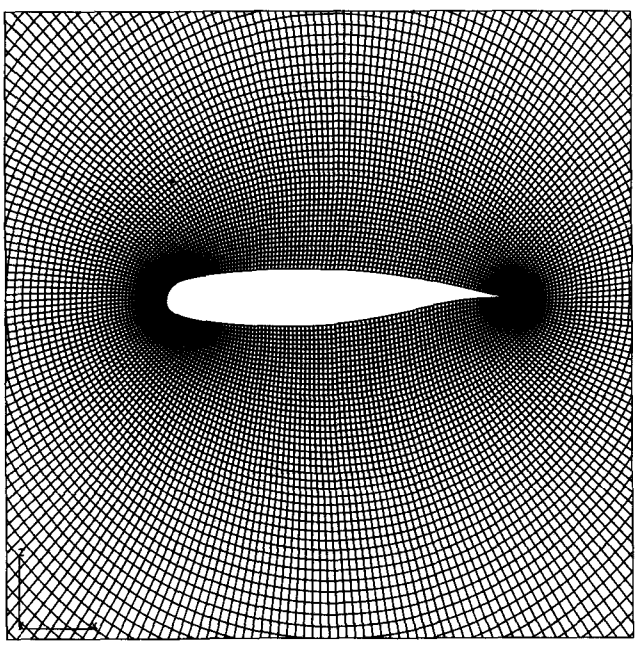

Fig. 3. Grid A around the NLR 7301 airfoil.

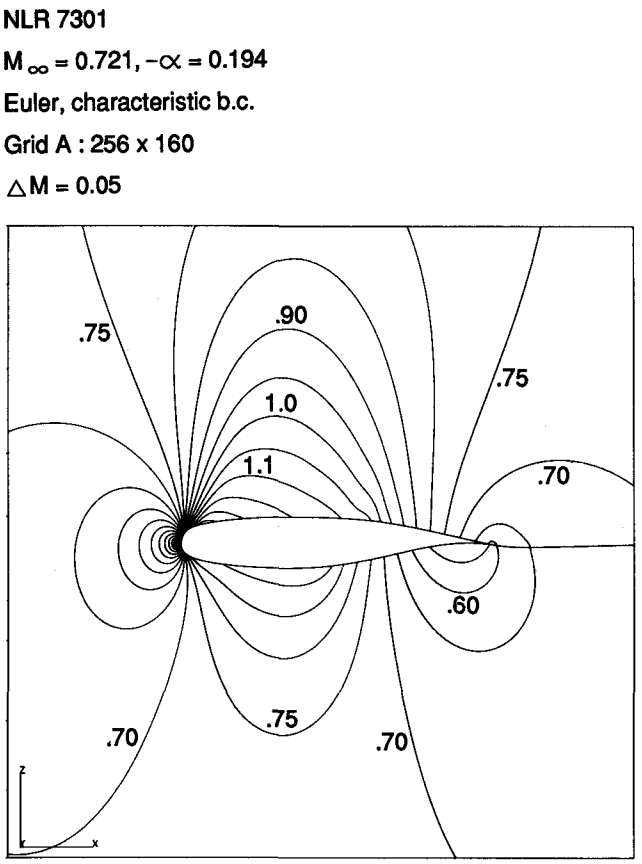

Fig. 4. Flow field Mach number contours.

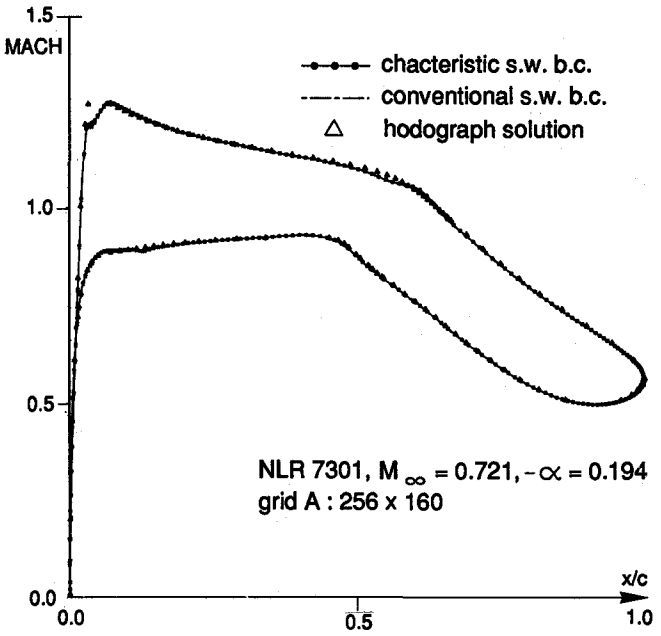

Fig. 6. Comparison of surface Mach number distribution with hodograph solution.

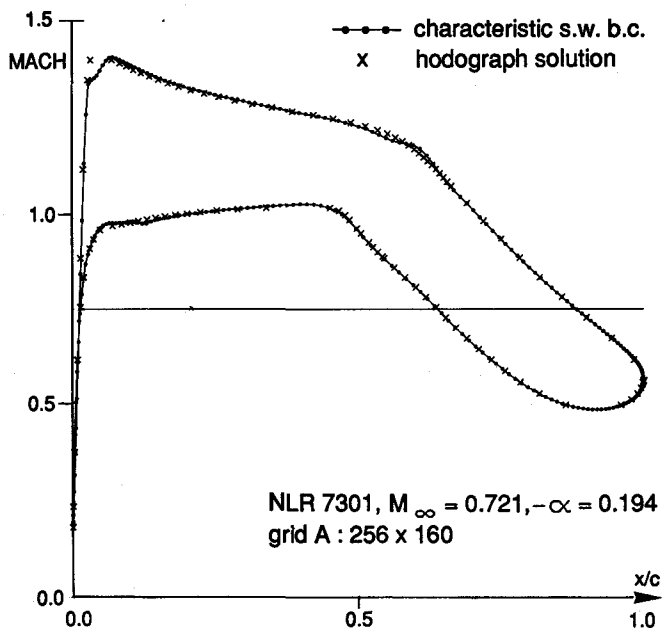

Fig. 5. Comparison of surface Mach number distribution.

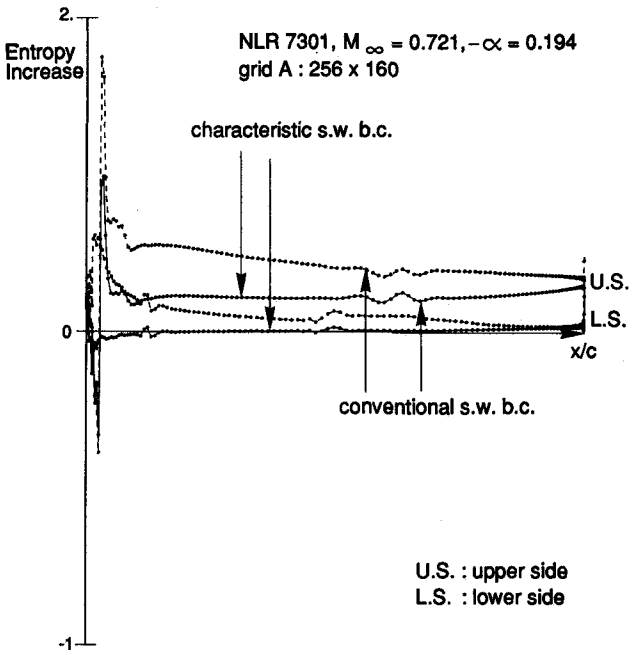

Fig. 7. Comparison of entropy increase along the surface.

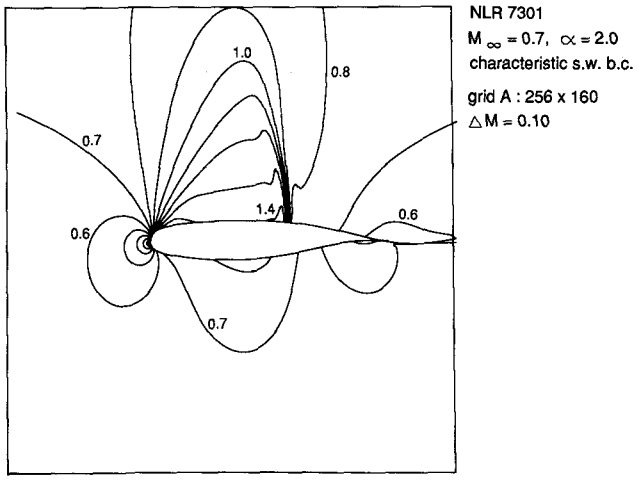

Fig. 8. Flow field Mach number contours.

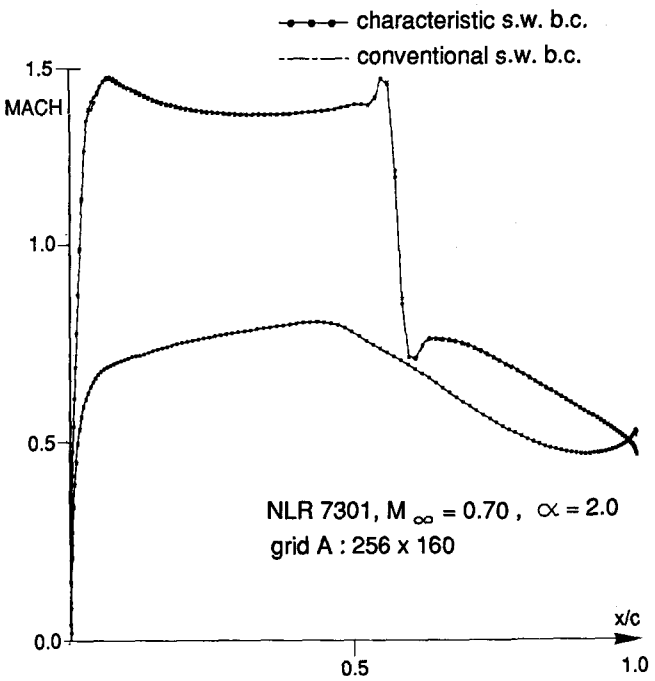

Fig. 10. Comparison of surface Mach number distribution.

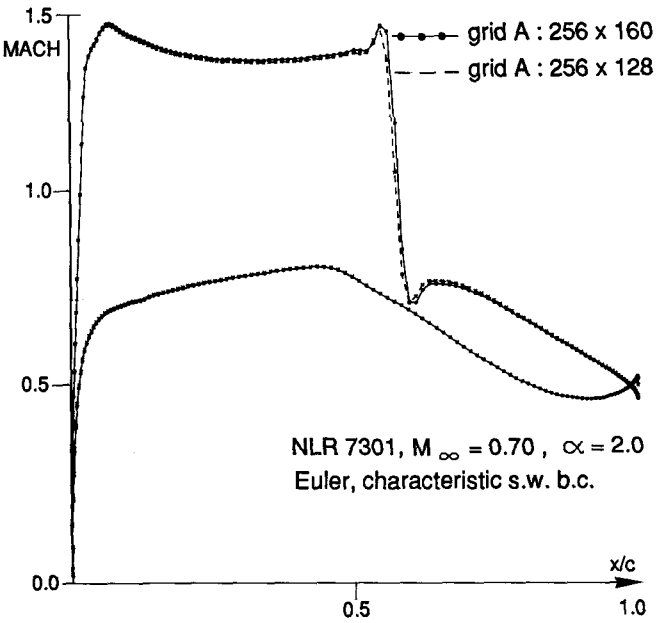

Fig. 9. Comparison of surface Mach number distribution.

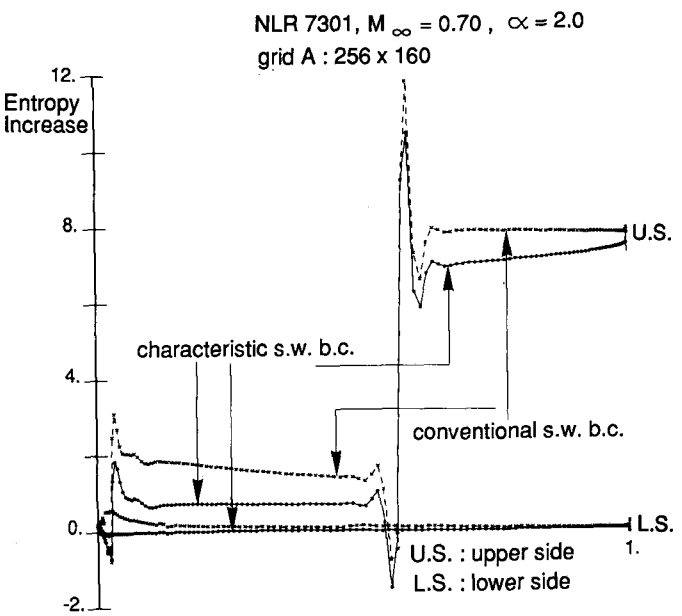

Fig. 11. Comparison of entropy increase along the surface.